Bioconjugate Chemistry

Article

pubs.acs.org/bc

Unique Surface Modification of Silica Nanoparticles with Polyethylenimine (PEI) for siRNA Delivery Using Cerium Cation Coordination Chemistry

Yekaterina Kapilov-Buchman,[†,§,#] Emmanuel Lellouche,[‡,§,#] Shulamit Michaeli,*[,‡,§] and Jean-Paul Lellouche*[,†,§]

[†]Department of Chemistry, Faculty of Exact Sciences, [‡]The Mina and Everard Goodman Faculty of Life Sciences, and [§]Institute of Nanotechnology and Advanced Materials, Bar-Ilan University, Ramat-Gan, 5290002 Israel

Supporting Information

ABSTRACT: The discovery of RNA interference (RNAi) as a naturally occurring mechanism for gene knockdown has attracted considerable attention toward the use of small interfering RNAs (siRNAs) for therapeutic purposes. The main obstacles of harnessing siRNAs as drugs are their inefficient delivery to cells and off-target effect making clinical applications very challenging. The positively charged, branched 25 kDa polyethylenimine (*b*-PEI) polymer is widely regarded as one of the most efficient nonviral commercially available transfection agents. However, it has also been shown that 25 kDa *b*-PEI is highly cytotoxic and can readily lead to cell death. In this specific context, this study presents the preparation and characterization of innovative 25 kDa *b*-PEI-decorated polycationic silica nanoparticles (SiO_2 NPs) for cellular siRNA delivery and subsequent gene silencing. A new method of *b*-PEI attachment onto the SiO_2 NP surface has been developed that makes use of cerium(III) cations (Ce^{3+}), a lanthanide group element, as an effective noncovalent inorganic linker between both polyNH$_2$−SiO_2 nanoparticle (SPA NPs) surface and polycationic 25 kDa *b*-PEI polymer. Two resulting novel SPA-Ce-PEI NPs consist of similar amounts of *b*-PEI, while possessing different amounts of Ce^{3+}. Various analytical techniques (TEM, DLS, ζ potential, ICP-AES, and TGA) have been used to deeply characterize NPs physicochemical qualities. The observed results of Ce^{3+}-dependent gene silencing and cytotoxic activities led us to conclusions about the role of Ce^{3+}-**N** bonding during the chemical attachment of the 25 kDa *b*-PEI shell onto the NP surface.

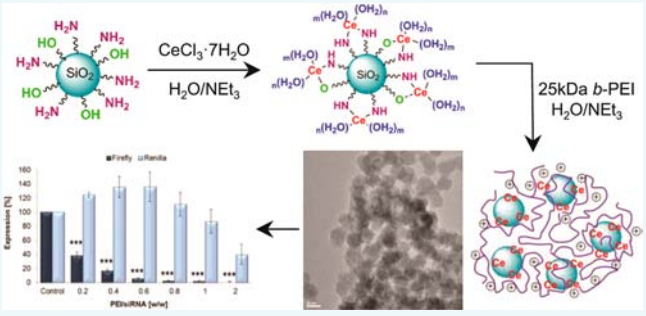

INTRODUCTION

RNA interference (RNAi) is initiated by small interfering RNAs (siRNA) with a length of 21 to 25 nucleotides, which participate in target-gene silencing by binding the RNA-induced silencing complex (RISC) to degrade complementary mRNA molecules.[1−3] During the past decade, this mechanism rapidly developed into a promising therapeutic strategy for a wide range of human diseases.[4] Although RNAi-based therapeutics offers tremendous potential to treat a wide variety of genetic disorders because of their highly potent and sequence-specific gene silencing activity,[5] the clinical use of siRNA for therapeutic purposes is still hampered.[6] There are several hurdles that limit the use of siRNA in clinical treatments: its ineffective systemic administration that comes as a result of instability and poor cellular uptake and off-target activity that can potentially lead to unwanted toxicities.[7,8]

Due to the natural negative charge of nucleic acids, a wide variety of cationic carriers, such as cationic lipids and polymers, have been extensively investigated to address problems involving in vitro and in vivo gene delivery through the formation of polyelectrolyte complexes between oppositely charged molecules.[9,10] Among cationic polymers, branched 25 kDa polyethylenimine (*b*-PEI) have shown to be efficient in protection and siRNA delivery.[11,12] The positively charged *b*-PEI has been used to electrostatically bind siRNAs, taking advantage of its strong positive charge. Most importantly, PEI has a strong capacity to mediate endosomal escape by the well-known "proton sponge" effect leading to the release of siRNA molecules into the cytoplasm.[13,14] Thus, the intracellular release of the PEI complexes from the lysosome may well contribute to the high transfection efficacies. Despite these favorable properties, high molecular weight and highly branched PEI polymers can cause cytotoxicity likely due to their positive charge.[15−17] For this reason, various chemical modifications by small molecules, neutral biocompatible polymers, and cross-linking have, recently, been proposed and vigorously investigated to reduce this highly limiting nonspecific

Received: February 16, 2015
Revised: March 29, 2015
Published: April 1, 2015

DOI: 10.1021/acs.bioconjchem.5b00100
Bioconjugate Chem. 2015, 26, 880−889

Scheme 1. Schematic Representation of Synthetic Steps towards SPA-Ce-PEI NPs

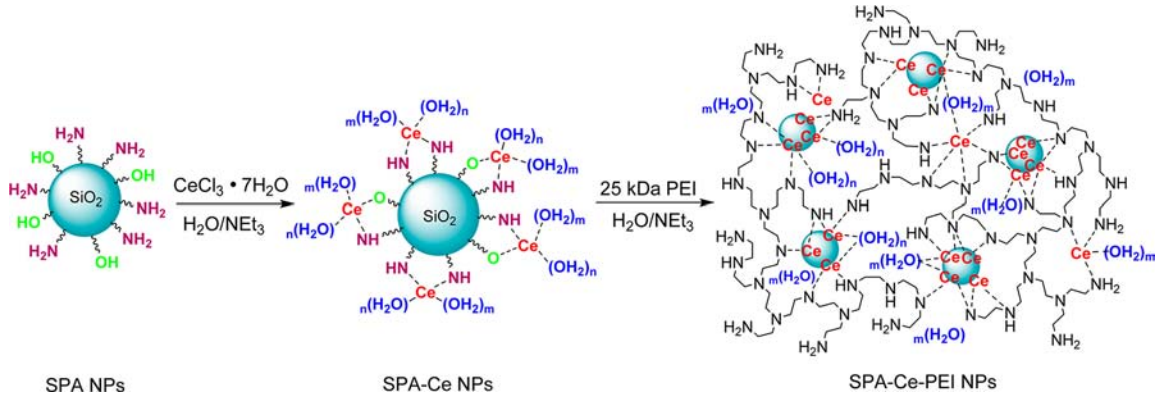

cytotoxicity while maintaining excellent polynucleic acid delivery and endosomal escape effectiveness.[18−23]

In this study, we introduce a chemical modification of *b*-PEI using multicoordinate chemistry of Ce^{3+} cations. Ce is a member of the lanthanide group elements and, thus, in its cationic 3/4+ states is able to establish coordination bonds with various organic and inorganic electron donors. Coordination numbers of the lanthanide cations normally are from 6 to 9 and bonding between lanthanide ions and coordinating ligands depends primarily on the electronegativity of the bonding atom in the ligand.[24−26] Bond formation follows the Lewis acid hardness order F^-, OH^-, H_2O, NO_3^-, $C1^-$, and so forth for monodentate ligands.[27] Complex formation with bidentate ligands in the presence of H_2O is usually successful only with ligands that form chelate rings through stronger Lewis base oxygen atoms, such as carboxylate anions (RCO_2^-) and *β*-diketonates ($RC(=O)-CH=C(O^-)R'$).[27] The added stability of resonating structures allows these ligands to compete successfully with OH^- or H_2O in the coordination sphere of the lanthanide cation. Ligands bonding through nitrogen or sulfur atoms normally cannot compete with H_2O for a position in the coordination sphere. Related complexes with lanthanides must be synthesized in nonaqueous media. However, since lanthanide cations are classified as hard acids,[24] it is not unreasonable that they form complexes with the lone pair of hard-base amines via ion−dipole interactions.[28] The stability of such complexes in H_2O is guaranteed by multifunctional coordination ligands that can coordinate metal center via multiple atoms and form polymetal−ligand complexes. Such a multifunctional coordination ligand role could be played by coordinating polymers and/or NP functional surfaces. For example, Belfiore et al. succeeded in significantly increasing the glass transition temperature of poly(vinylamine) by adding M(III) cations from the first row of the f-block (metals from lanthanum to lutetium) at pH 9−10 in aqueous media.[29] The enhancement in the glass transition temperature was explained in terms of multifunctional coordination cross-linking. Herein, this study discloses the formation of new nanomaterials (NMs) that involve unusual bonding between Ce^{3+} and chelating polyamines in aqueous media without using any *organic* coupling reagent. Thus, such unique linkage chemistry is promoting (i) a new approach dealing with *b*-PEI attachment onto the SiO_2 NPs surface for siRNA delivery applications, as well as (ii) an original attempt to mitigate polycationic *b*-PEI cytotoxic effects by reducing its free amine amount available for interaction with cells.

More specifically, $CeCl_3{\cdot}7H_2O$ was used to coordinately bind with amines in basic conditions to receive Ce- and 25 kDa *b*-PEI-modified silica nanoparticles (SiO_2 NPs). Such NPs were made of both 25 ± 3 nm polyNH$_2$−SiO_2 (SPA) NPs and 25 kDa *b*-PEI phases that were interconjugated by Ce^{3+} atom coordination resulting in SPA-Ce-PEI NPs. The resulting functional NPs were analyzed by various physical and analytical methods and their gene-silencing in vitro capability was tested as well. During the course of this study, a relationship between Ce surface concentration and two cellular activities (gene silencing versus cytotoxicity) have been explored. To conclude that siRNA-mediated silencing indeed occurs due to the presence of *b*-PEI, additional nanomaterial species were also tested, including SPA NPs only and SPA with Ce^{3+}only, SPA-Ce NPs.

RESULTS AND DISCUSSION

Synthesis of SPA-Ce-PEI NPs. SPA NPs were synthesized using the well-studied and previously described Stöber method[30] (tetraethyl orthosilicate hydrolysis and condensation reactions using NH_4OH basic catalysis in an EtOH solution) with subsequent addition of aminopropyltriethoxysilane (APTES) that resulted in 25 ± 3 nm SiO_2 NPs that possess a polyaminated (polyNH$_2$) functional shell.[31] Thereafter a series of Ce^{3+}-modified SPA NPs was readily prepared by adding different amounts of $CeCl_3{\cdot}7H_2O$ to a constant amount of SPA NPs in aqueous media in the presence of NEt_3 (Scheme 1). $CeCl_3{\cdot}7H_2O$ amounts were determined by various molar percentages of $-NH_2$ groups present on SPA NPs (0.5 mmol/g) as quantified by a Kaiser Test.[32] This synthetic step resulted in a two nanoparticulate systems that possessed different molar percentages of Ce (20 and 60%) compared to N that comes from APTES functionalized surface. After several washes from dissolved byproducts using centrifuge precipitation (12 min, 19 500 *g*-force, 4 °C), NP decoration with the 25 kDa *b*-PEI took place. This step was performed by simple mixing of freshly prepared SPA-Ce NPs with 20 w% of PEI (aqueous solution, 0.4 mM) in the presence of NEt_3 in H_2O. That process resulted in a series of PEI-decorated SPA-Ce NPs.

Size, Shape, and ζ Potential. Figure 1 represents TEM micrographs of the starting material (SPA NPs) and of two Ce- and PEI-decorated SPA-Ce-PEI NPs. SPA NPs have an elliptical shape with an average long axis size of 25 ± 3 nm (150 NPs were measured from TEM images using *ImageJ* software). After treatment with Ce^{3+}cations and *b*-PEI, surface of some NPs looks to have some contrasting centers and resembles prickly pears (Figure 1B,C). Another form of the

DOI: 10.1021/acs.bioconjchem.5b00100
Bioconjugate Chem. 2015, 26, 880−889

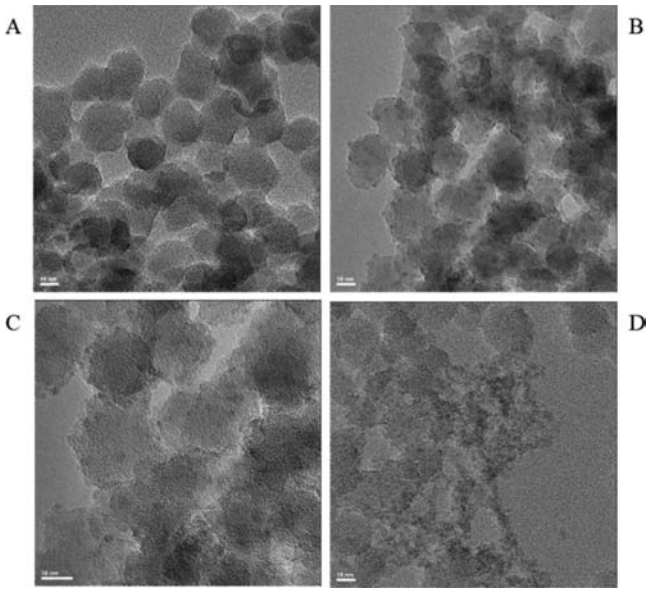

Figure 1. TEM micrographs of (A) SPA, (B,C) SPA-Ce_{20}-PEI, and (D) SPA-Ce_{60}-PEI NPs. The scale bar represents 10 nm in all images.

modification appears as a web-like material bridging between closely located NPs (Figure 1D).The origin of this matter comes from the presence of two components. On the one hand, heavy Ce^{3+} cations have a good probability of capturing electrons and appearing darker in TEM images than smaller atoms. On the other hand, PEI is an organic polymer possessing a low density and could not be seen in TEM micrographs unless it is mixed with a more TEM/electron contrasting material. Thus, the web-like material on the NP surface is probably relating to Ce^{3+}cations chelated by PEI chains. The more Ce is used in NP preparation, the more contrasted the cross-linked polymer web appears in micrographs, which fully supports the NP surface chemical manipulation.

DLS and ζ potential measurements were performed for all (starting, intermediate, and final) materials using dilute 0.05 mg NPs/mL aqueous dispersions (Table 1). The values of hydrodynamic diameters are represented by a number distribution, namely, the size of the major colony in dispersion. The polydispersity index (PdI) values were also given to more accurately understand colloidal behavior of the studied systems. A low (reaching zero) PdI value is an indication of a rather stable monodispersed colloidal system, while a high value (close to 1) indicates a high polydispersity and aggregation of NPs. The starting, SPA, and the intermediate, SPA-Ce NPs, form unstable and aggregating colloidal systems where the diameters of the majority of NPs fall in the range of 989−1813 nm. The final SPA-Ce-PEI NPs behave like much more stable suspensions forming loose aggregates with variable hydrodynamic diameters depending on NP type. The sample containing 20% Ce^{3+}, the SPA-Ce_{20}-PEI NPs, demonstrates the most abundant average size of 324 ± 8 nm (PdI = 0.37). SPA-Ce_{60}-PEI NPs are smaller with 236 ± 17 nm hydrodynamic average size (PdI = 0.17).

Table 1. DLS and ζ Potential Values Measured at ∼0.05 mg/mL Concentration in Deionized H_2O

NP type	DLS [nm]	PdI	ζ potential [mV]
SPA	1244 ± 318	0.64	+24.7
SPA-Ce_{20}	1813 ± 614	0.42	+21.7
SPA-Ce_{60}	989 ± 102	0.22	+17.9
SPA-Ce_{20}-PEI	324.3 ± 7.9	0.37	+34.9
SPA-Ce_{60}-PEI	236.0 ± 17.3	0.17	+23.6

There is a significant deviation between SPA NP size demonstrated by TEM and DLS. This fact is due to a high surface tension of SPA NPs that comes as a result of surface chemistry, which is not able to stabilize such small particles. The presence of acidic silanol (−Si−OH) and basic primary amino- ($-NH_2$) groups on SPA NPs surface destabilizes their aqueous suspension. Formation of hydrogen and electrostatic bonds occurs between these reversely charged surface groups, results in severe aggregation. After attachment of Ce^{3+} the hydrodynamic behavior changes differently in each case. SPA-Ce_{20} NPs show even greater instability than SPA NPs, but addition of more Ce^{3+} as in SPA-Ce_{60} slightly decreases the aggregation. When *b*-PEI is added onto NPs surface a total colloidal stability is increased due to high hydrophilicity of this polymer that forms hydrogen and electrostatic bonds with H_2O. The clustering of aggregated NPs is reduced when *b*-PEI comes between two groups of NPs. On the other hand, a cross-linking effect probably takes place in the formation of a new polymer shell. "Coordination cross-links" occur when amines displace H_2O molecules in the first coordination shell and the lanthanide forms a complex with at least two amines on different chains. Unfortunately, this phenomenon promotes NPs aggregation by binding different NPs into the same cluster, preventing their separation despite a hydrophilic NPs profile.

SPA NPs show a positive ζ potential of 24.7 mV due to protonable polyamine surface. After coordination with Ce^{3+}, a reduction in positive ζ potential was recorded that was proportional to the Ce^{3+} amount. Namely, a higher Ce^{3+} amount caused a more significant loss of positive charge showing only a 17.9 mV value for SPA-Ce_{60} NPs. This reduction in surface charge is explained by a decreasing amount in free primary amines that are no longer protonable and thus not positively charged. After PEI attachment, the positive charge of SPA-Ce NPs increased inversely to the Ce^{3+} amount, showing a 34.9 mV ζ potential value, for SPA-Ce_{20}-PEI NPs, and a 23.6 mV one for SPA-Ce_{60}-PEI NPs. This trend fully matches our expectations, as at high Ce^{3+} amounts, more PEI amines undergo functional cross-linking while being no longer available for protonation (positive charge reduction). This overall phenomenon is clearly reflected by the observed ζ potential values.

Inductively Coupled Plasma. Inductively coupled plasma atomic emission spectroscopy (ICP-AES) technique was then used to quantify the weight percentage of elemental Ce in each NM. Obtained results fully supported our expectations about contacting Ce quantities used in SPA-Ce-PEI NPs. Table 2 describes (i) amounts of Ce used for the preparation of each

Table 2. Ce Weight Percentages: Calculated (Theoretical) and Measured Values (ICP-AES)

NP type	(i) Ce [μmol/100 mg NPs]	(ii) % Ce (calc. value) [w/w]	(iii) % Ce (ICP) [w/w]
SPA-Ce_{20}-PEI	10	1.40	1.18
SPA-Ce_{60}-PEI	30	4.20	3.50

DOI: 10.1021/acs.bioconjchem.5b00100
Bioconjugate Chem. 2015, 26, 880−889

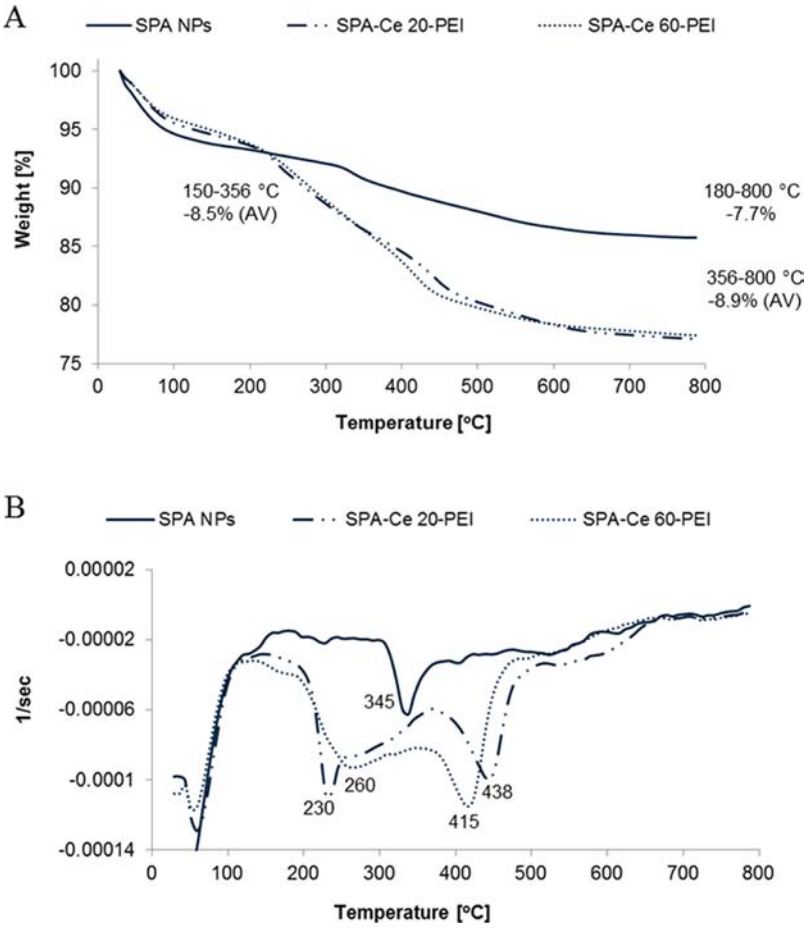

Figure 2. (A) Weight loss (TGA) and (B) first derivative (DTG) curves of SPA and SPA-Ce-PEI NPs.

batch, (ii) calculated, and (iii) experimentally (ICP-AES)-measured weight percentages of Ce atoms. Calculations were based on amounts of $CeCl_3 \cdot 7H_2O$ that were used in reacting 100 mg SPA NPs with a relevant amount of Ce^{3+} cations. A great degree of consistency between both theoretical and experimental results demonstrates well-chosen synthetic conditions and a reliable level of accuracy.

Thermogravimetric Analysis (TGA). Weight amounts of the organic PEI component in fully functional SPA-Ce-PEI NPs have been quantified using thermogravimetric analysis (TGA). Weight loss tracking involved the starting SPA and subsequent SPA-Ce-PEI NPs with 20 and 60 mol percentage Ce^{3+} (Figure 2). Such TGA analyses have been conducted in the temperature range of 25−800 °C under airflow (full burn conditions) using a 10 °C/min increasing temperature profile. Quantification of APTES and PEI contents were calculated by taking into account weight losses after thermal decomposition.

Corresponding weight loss graphs show a two-step profile for SPA and three-step profile for all the SPA-Ce-PEI NPs as defined by the number of major minimum points of first derivative (DTG) curves for each NP material. Table 3 details the observed weight losses for each NM and the final calculated PEI weight percentages. The first step (25−180 °C range for SPA NPs and 25−150 °C range for SPA-Ce-PEI NPs) weight loss corresponds to evaporation of adsorbed (not coordinated) moisture and constitutes about 5.1−6.6 wt % loss, depending on NP type (Table 3, first step). Weight loss step relating to APTES decompositions took place at 345 °C as demonstrated by a minimum point at DTG curve of SPA NPs (Figure 2B).

Table 3. Temperature-Dependent TGA Weight Loss Steps with Quantified Data

NP type	first step	second step	third step	PEI [%]
SPA[a]	6.6	7.7	---	---
SPA-Ce_{20}-PEI[b]	5.4	8.3	9.1	9.7
SPA-Ce_{60}-PEI[b]	5.1	8.7	8.7	9.8

[a]Ending of the first step and beginning of the second was at 180 °C. [b]Ending of the first step and beginning of the second was at 150 °C, and ending of the second step and beginning of the third at 356 °C.

After PEI decoration the decomposition profiles change dramatically showing two major minima at 230 and 415 °C for SPA-Ce_{20}-PEI NPs and 260 and 438 °C for SPA-Ce_{60}-PEI NPs. According to these definitions a weight loss due to APTES decomposition in SPA NPs made 7.7% (180−800 °C range). The second and third weight loss stages of SPA-Ce-PEI NPs include combustion of both APTES and PEI components. The total PEI amount constituting SPA-Ce-PEI NPs could be readily calculated by subtracting the second weight loss step of SPA NPs (combustion of APTES, 7.7%) from the sum of second and third weight loss stages of the SPA-Ce-PEI NPs profile (APTES and PEI decompositions). This method of PEI quantification excludes weight loss contributions from any adsorbed moisture and/or volatile reagent(s) from the first step. In this manner, the calculated weight amounts for the PEI phase have been found to be similar (9.7 and 9.8 wt %, Table 3) in both SPA-Ce-PEI NPs (average 9.75 wt %, Figure 2A).

DOI: 10.1021/acs.bioconjchem.5b00100
Bioconjugate Chem. 2015, 26, 880−889

Characterization of SPA-Ce-PEI/siRNA Polyplexes by DLS and ζ Potential Measurements. Positively charged SPA-Ce-PEI NPs are readily attached with negatively charged siRNA by electrostatic conjugation and form polyplexes with variable SPA-Ce-PEI/siRNA weight ratios (Figure 3). In order to compare two different SPA-Ce-PEI NPs, we used common units that characterized by PEI to siRNA weight contents (Figure 3). PEI weight was calculated by multiple of its weight fraction found by TGA and the total NP dispersion concentration. The corresponding samples were prepared using variably increasing w/w PEI/siRNA ratios in the 0.2–2.0 range. To obtain the size and ζ potential of SPA-Ce-PEI/siRNA polyplexes of different weight ratios, the samples were prepared by contacting a constant amount of SPA-Ce-PEI NPs (50 μg) with variably decreasing amounts of siRNA in deionized H_2O (15 min incubation) and subsequently diluting with H_2O up to 1 mL to obtain constant (0.05 mg/mL) NP-concentration suspensions. Size and ζ potential were measured for each sample in triplicate repetition mode.

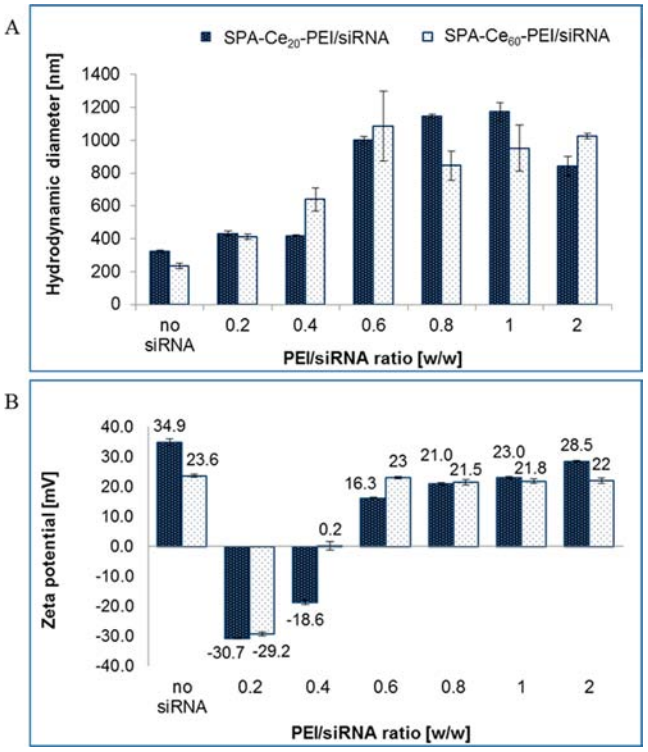

Figure 3. (A) Hydrodynamic diameters and (B) ζ potentials of SPA-Ce-PEI NPs/siRNA polyplexes at different PEI/siRNA w/w ratios.

The hydrodynamic diameters of both SPA-Ce-PEI NPs are smallest before complexation with siRNA. The polyplex DLS size increases with increasing PEI/siRNA weight ratio for both NPs tested until there is no more increase. This point is different for the two NPs, with 1.0 PEI/siRNA w/w ratio for SPA-Ce_{20}-PEI and 0.6 PEI/siRNA w/w ratio for SPA-Ce_{60}-PEI NPs (Figure 3A). ζ Potential values also demonstrate some similarities and differences between these two NPs (Figure 3B). The samples without siRNA demonstrate positive surface charges where their values depend on Ce^{3+} content (34.9 and 23.6 mV for "Ce_{20}" and "Ce_{60}", respectively). While at 0.2 PEI/siRNA w/w ratio, samples with the highest siRNA content, ζ potential values turn out to be negatively charged (around −30.0 mV). In general, as the siRNA mass fraction reduces the ζ potentials from negative to positive again with some differences between the two kinds of SPA-Ce-PEI NPs. At 0.4 PEI/siRNA w/w ratio, SPA-Ce_{20}-PEI NPs still have negative surface charge (−18.6 mV), while SPA-Ce_{60}-PEI NPs neutralize all the negative charge coming from siRNA demonstrating near zero ζ potential. Another expression of such fast negative charge neutralization is seen further comparing the two NP systems. NPs with the higher Ce^{3+} content (Ce_{60}) reach their maximal original ζ potential (around 23 mV) at 0.6 PEI/siRNA ratio, while NPs with lower Ce^{3+} content (Ce_{20}) only slightly approach their original positive charge (28.5 vs 34.9 mV) at the highest PEI/siRNA ratio of 2.0. This behavior can be addressed to additional interactions between SPA-Ce-PEI NPs and siRNA. It is probably that siRNA attaches not only by electrostatic forces but also by a complexation of phosphate backbones with Ce^{3+} in coordinating chemistry. This type of complexation neutralizes the

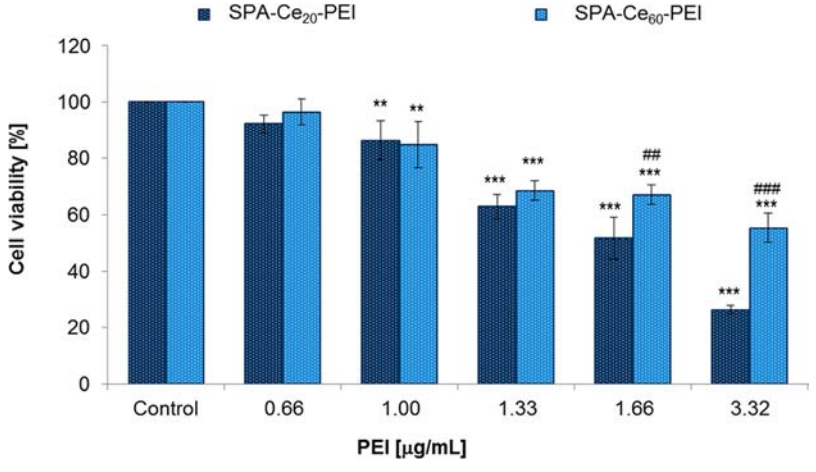

Figure 4. Toxicity of SPA-Ce-PEI/siRNA and free 25 kDa *b*-PEI/siRNA polyplexes by MTT using U2OS-Luc cells. U2OS-Luc cells (1×10^4 cells/well) were treated with different amounts of SPA-Ce-PEI/siRNA and free 25 kDa PEI/siRNA polyplexes. After 48 h incubation, the medium was removed and replaced with fresh containing MTT. Adsorption values were measured at 570 nm and normalized to the control (untreated) sample. Data are expressed as mean ± SD of three different experiments based on a two way ANOVA with multiple comparison Bonferroni post hoc analysis ($^{**}p < 0.01$, $^{***}p < 0.001$ vs control, $^{\#\#}p < 0.01$, $^{\#\#\#}p < 0.001$ vs SPA-Ce_{20}-PEI).

DOI: 10.1021/acs.bioconjchem.5b00100
Bioconjugate Chem. 2015, 26, 880–889

negative charge of phosphate oxygen that contributes its lone pair of electrons to form Ce^{3+}-**O** bond.

In our previous work[31] we prepared 25 kDa *b*-PEI-functionalized SPA NPs for gene silencing by its covalent attachment using a divinyl sulfone ($(CH_2{=}CH)_2SO_2$) linker. In that work, the ζ potential profile looked similar to those obtained in this study, but when using a much higher range of PEI/siRNA ratios (1.0−20.0). For example, the turning point from negative to positive ζ potential occurs between 1.0 and 2.0 PEI/siRNA ratio for SPEI NPs. It means that in order for NPs to complex with the same amount of siRNA, it should be present in much greater ratio than in SPA-Ce-PEI NPs. By comparing these two works it can be concluded that Ce^{3+} has a great effect on the complexation with siRNA.

Cytotoxicity Tests. MTT assays measure the ability of cells to reduce the tetrazolium dye, MTT, to insoluble formazan resulting in a purple color. Since this requires functioning mitochondria, these MTT assays effectively measure the metabolic activity of live cells. The cytotoxicity of the SPA-Ce-PEI/siRNA polyplexes was determined in the dual-luciferase expressing (Firefly/*Renilla*) human osteosarcoma U2OS cell line (U2OS-Luc) by MTT-based cell viability assay after 48 h incubation (Figure 4). MTT tests have been also conducted for PEI-free NPs, i.e., SPA and SPA-Ce_{60} NPs, for free 25 kDa *b*-PEI and for Ce^{3+} cations in order to differentiate between cytotoxicity coming from NPs, PEI, and Ce^{3+} (Figures S3−S5, see SI). The horizontal axis was chosen to be represented by increasing PEI/siRNA w/w ratios that enable the formation of silencing polyplexes in the 0.4−2.0 PEI/siRNA w/w ratio range using a constant 100 nM siRNA amount (Figure 4). The PEI-free NPs were taken with the same NP concentration as SPA-Ce-PEI NPs (for unit conversion see Table 4). Table 4 represents conversion of PEI/siRNA weight ratios to the widely usable N/P ratios (nitrogen of PEI/phosphate of siRNA), to NP/siRNA ratios (total NP weight/siRNA weight), and also to PEI, NPs, and Ce concentrations in μg/mL units. All these MTT results were compared to the ones obtained with untreated cells.

Table 4. Conversion of PEI/siRNA wt % Values to Atomic N/P Ratios, NP/siRNA wt % Values, PEI, NPs, and Ce Weight Concentrations (μg/mL)

PEI/siRNA [w/w]	N/P	NP/siRNA [w/w]	PEI [μg/mL]	NPs [μg/mL]	Ce [μg/mL]
0.2	1.46	2.06	0.33	3.4	0.12
0.4	2.92	4.12	0.66	6.8	0.24
0.6	4.38	6.18	1.00	10.3	0.36
0.8	5.84	8.24	1.33	13.7	0.48
1.0	7.3	10.30	1.66	17.1	0.60
2.0	14.6	20.60	3.32	34.2	1.20

From Figure S3, it arises that SPA and SPA-Ce_{60} NPs (without PEI) did not cause any toxicity to cells within the tested ratios range, while SPA-Ce-PEI NPs behave totally different (Figure 4). No significant toxicity can be seen using a PEI/siRNA w/w ratio of 0.4, while a ratio of 0.6 resulted in minor toxicity of ∼15% in cells treated with both NPs. Higher ratios lead to an increase in the toxicity in both NPs; however, cells treated with SPA-Ce_{20}-PEI NPs showed a significantly higher toxicity than those with a 60% Ce^{3+} content (73.61% and 44.74%, respectively, with a PEI/siRNA w/w ratio of 2.0). This difference can be explained due to the higher Ce^{3+} surface concentration of the SPA-Ce_{60}-PEI NPs that makes tighter conjugation to PEI, resulting in fewer amine functions available for interaction with cell contents. Free PEI treatment at different concentrations (Figure S4) corresponding to those used for the silencing experiments results in a toxicity of around 20% with the highest PEI concentration of 3.32 μg/mL. However, no efficient silencing can be observed using this concentration. In addition and quite interestingly, free Ce^{3+} cations did not show any relevant U2OS-Luc cellular toxicity as a separate NPs surface engineering component (MTT assay, Figure S5, Supporting Information (SI) section).

Endocytosis and siRNA delivery by SPA-Ce-PEI NPs. The cellular uptake of SPA-Ce_{60}-PEI/FITC-siRNA polyplexes was confirmed using fluorescent confocal microscopy (Figure 5). In this study, we used fluorescent FITC-labeled siRNA bound to SPA-Ce_{60}-PEI NPs using a 0.6 PEI/siRNA w/w ratio, which demonstrated no major cytotoxicity by MTT (Figure 4) and efficient silencing in the dual-luciferase assay (Figure 6). As we can see in Figure 5A−D, SPA-Ce_{60}-PEI/FITC-siRNA polyplexes (green dots) efficiently penetrate U2OS-Luc cells and are located in the cytoplasm around cell nuclei (blue). A 3D fluorescence-based image of a single cell has been generated using a set of 2D sectional subimages (*z* stacking) obtained by confocal microscopy (*Imaris* software, Figure 5E,F). It is clearly shown by 3D microphotograph that the green fluorescence signals appear around (Figure 5E) and above (Figure 5F) the cell nucleus evidencing an efficient SPA-Ce_{60}-PEI/FITC-siRNA polyplexes cellular uptake. In addition, the 3D imaging shows no fluorescence within the nucleus, meaning that SPA-Ce_{60}-PEI/siRNA polyplexes cannot penetrate cell nuclei probably due to their large size as demonstrated in Figure 3.

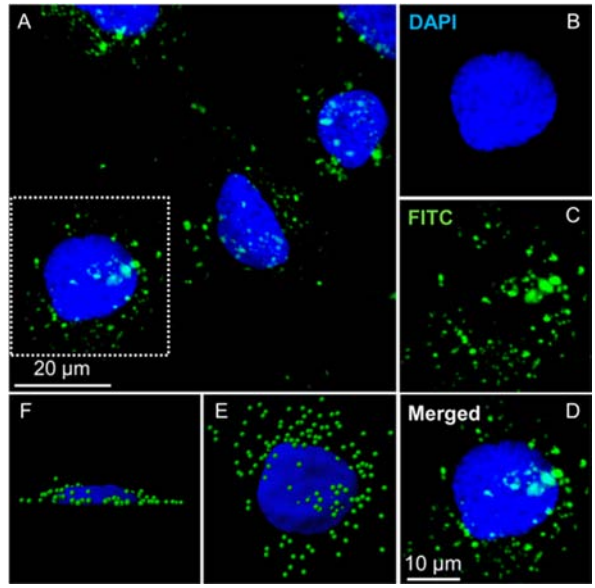

Figure 5. Penetration of SPA-Ce_{60}-PEI/FITC-siRNA polyplexes to U2OS-Luc cells. U2OS-Luc cells (1×10^5 cells/well) were transfected with SPA-Ce_{60}-PEI/FITC-siRNA polyplexes (50 nM) at a 0.6 PEI/siRNA w/w ratio. After 24 h, cells were fixed, and nuclei were stained with DAPI (blue). Images were taken with a Leica TCS SPE (63×) Confocal Laser scanning microscope (CLSM), and then the 3D images (E,F) were edited using *Imaris* software (Bitplane).

Gene silencing tests were performed using human osteosarcoma U2OS cells stably expressing the Firefly/*Renilla* luciferases (U2OS-Luc). The dual-luciferase system enables

DOI: 10.1021/acs.bioconjchem.5b00100
Bioconjugate Chem. 2015, 26, 880−889

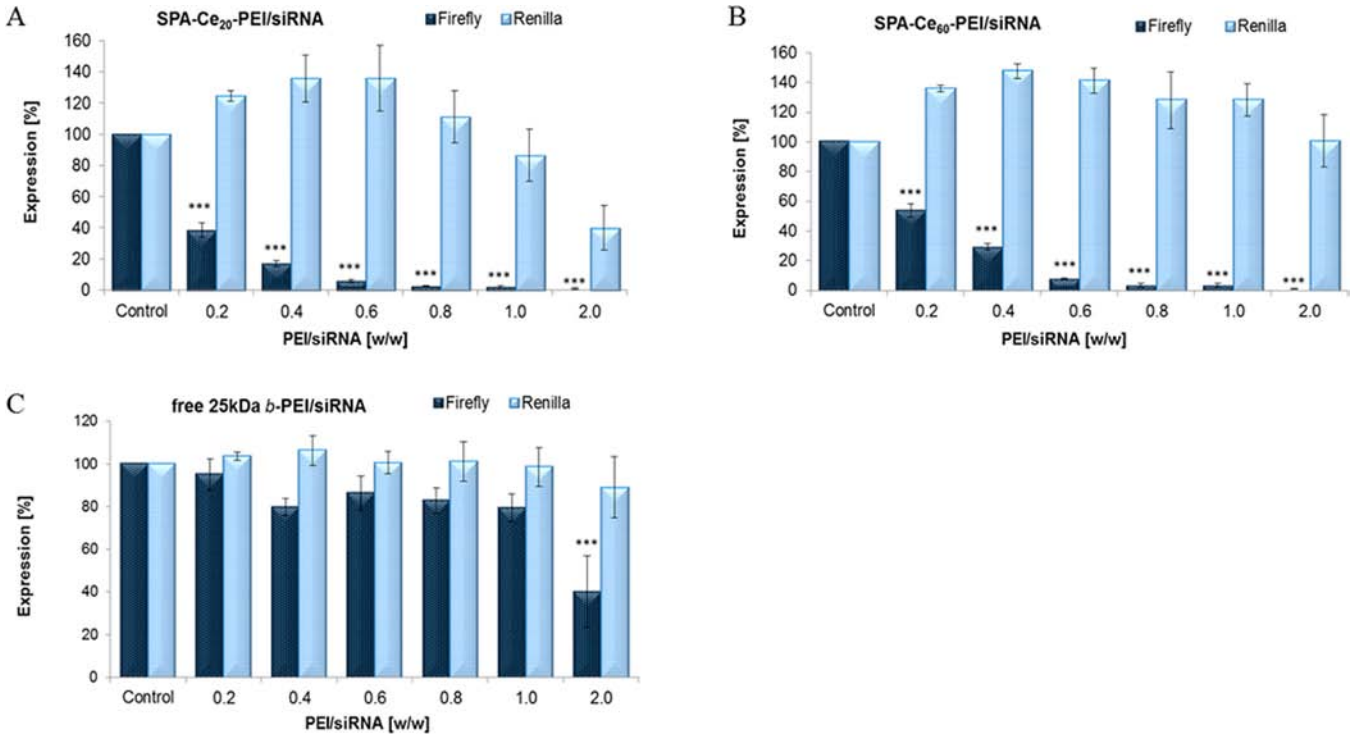

Figure 6. siRNA delivery to U2OS-Luc cells. U2OS-Luc cells (1×10^4 cells/well) were transfected with Firefly luciferase siRNA (0.166 μg, 100 nM) mixed with SPA-Ce-PEI NPs at different PEI/siRNA w/w ratios. After 48 h, cells were assayed for both Firefly and *Renilla* luciferase activities using a Dual-GLO Luciferase Assay System. Silencing efficacy is denoted by luciferase activity normalized to control (untreated cells) luciferase activity. Data are expressed as mean ± SD of three different experiments according to the results of a two way ANOVA with multiple comparison Bonferroni post hoc analysis (***$p < 0.001$ vs control Firefly).

measuring the specific silencing of Firefly luciferase, whereas the *Renilla* remains unchanged unless tested NPs caused toxicity and cell death. U2OS-Luc cells were incubated with SPA-Ce-PEI/siRNA polyplexes at a constant 100 nM (166 ng) siRNA concentration using six different w/w PEI/siRNA ratios (0.2, 0.4, 0.6, 0.8, 1.0, and 2.0). Figure 6 represents gene expressions after treating the cells with Firefly specific siRNA polyplexes of three different materials: SPA-Ce_{20}-PEI and SPA-Ce_{60}-PEI NPs (Figure 6A,B, respectively) and free 25 kDa *b*-PEI (Figure 6C). All enzyme levels were compared to control (untreated cells).

The most prominent results shown by these tests are the significant gene silencing by extraordinarily low PEI/siRNA w/w ratios of both SPA-Ce-PEI/siRNA polyplexes (Figure 6A,B). Table 4 shows PEI/siRNA w/w ratios converted to corresponding atomic N/P ratios. Usually, in other works, a significant gene silencing takes place at a 10−20 N/P ratio range when using various PEI-based nanovectors.[33−36] In our case, a significant reduction in the Firefly luciferase expression (61.5% and 46.1% for Ce_{20} and Ce_{60}, respectively) already takes place at a lowest 0.2 PEI/siRNA w/w ratio, which corresponds to a 1.46 N/P ratio (for unit conversion see Table 4). Other characteristics can be addressed to the difference between these two Ce^{3+}- and PEI-functionalized NPs. SPA-Ce_{20}-PEI NPs with a surface Ce^{3+} content of 20% demonstrate better silencing capacities than SPA-Ce_{60}-PEI NPs especially at low PEI/siRNA w/w ratios of 0.2 and 0.4 with a reduction of 83.2% versus 70.7% (Ce_{20} and Ce_{60}, respectively) at the 0.4 ratio. Also, at high PEI/siRNA w/w ratios (1.0−2.0) reduction in *Renilla* levels, demonstrated by SPA-Ce_{20}-PEI/siRNA polyplexes, points to some cytotoxicity. According to the *Renilla* levels no toxicity was observed from SPA-Ce_{60}-PEI/siRNA polyplexes. However, compared to the previously described MTT results both SPA-Ce-PEI NPs cause toxicity, especially at high PEI/siRNA weight ratios. The inconsistency between these results can be explained by the way each assay measures cell toxicity. MTT assay is based on the reduction of the tetrazolium salt by active mitochondria only in live cells, and therefore this assay is more sensitive than the dual-luciferase assay which measures *Renilla* levels in all cells unless they undergo lysis. Despite the higher MTT assay sensitivity, SPA-Ce_{60}-PEI NPs apparently can cause less lysis than SPA-Ce_{20}-PEI NPs. This statement is fully consistent with our expectations, since more Ce^{3+} on the surface makes more cross-links to PEI reducing both toxicity and gene silencing capacity due to a decrease in its "proton sponge" effect strength.

Comparing silencing efficiency of SPA-Ce-PEI NPs with free unconjugated 25 kDa *b*-PEI (Figure 6C) demonstrates a significant difference in potency PEI/siRNA ratios for gene silencing. No efficient gene silencing occurs at PEI/siRNA ratios lower than 2.0. It means that the modified/attached PEI phase as in SPA-Ce-PEI NPs is much more potent for down regulation than the free one. A likely explanation for this interesting phenomenon arises from chemical considerations. Indeed, Ce^{3+} cations involved in the design of these nanovehicles add an additional type of bonding (Ce lanthanide coordination chemistry)[25,26] between the particle carrier and its siRNA component. The coordinating nature of shell Ce^{3+} cations/complexes enables dynamic partial breaking of Ce^{3+}−**N** (PEI) bonds by forming new thermodynamically more stable Ce^{3+}−**O**P═O$(OR)_2$ bonds when reacting with such hard Lewis bases, i.e., siRNA polyphosphate backbone species.

DOI: 10.1021/acs.bioconjchem.5b00100
Bioconjugate Chem. 2015, 26, 880−889

Therefore, and due to this coordinative participation in siRNA attachment/complexation, the formation of stable NP-based polyplexes with siRNA species will necessitate lower amounts of *b*-PEI when compared to traditional free *b*-PEI-siRNA polyplexes.

SPA-Ce_{60} NPs without a *b*-PEI shell were also tested in gene silencing using the same amounts of NPs to produce polyplexes with siRNA using the same NP/siRNA w/w ratios as in SPA-Ce-PEI systems (Figure S6A, see SI). If Ce^{3+} can complex siRNA maybe SPA-Ce NPs are able to deliver siRNA to cytosol avoiding use of cytotoxic PEI. Figure S6A shows that no silencing occurs when using PEI free NPs. We also tested NPs without PEI, but with polyamine surface, the SPA NPs, in gene silencing assay (Figure S6B). Despite a high quantity of primary amines on the NP surface, there is no silencing effect at the tested NP/siRNA ratios that are analogous to amounts of NPs that form 0.2−2.0 PEI/siRNA polyplexes. This data confirms that for a significant gene silencing a highly protonatable compound like *b*-PEI must be present on the transfection agent. The presence of only primary amines close to the NP surface and/or a coordinating agent on the nanovehicle are not sufficient conditions for effective siRNA delivery.

■ CONCLUSIONS

In this study, we introduced a new concept of NP surface modification using the rich coordination chemistry of nontoxic Ce^{3+} cations/complexes. In this regard, the $CeCl_3{\cdot}7H_2O$ salt has been used as a metal linker between both SiO_2 polyamine surface and 25 kDa *b*-PEI for the production of corresponding nanocomposites for siRNA delivery. We compared two types of Ce^{3+}- and PEI-modified SPA-Ce-PEI NPs in in vitro gene silencing testing. We found that using Ce^{3+} cations/complexes on the NPs surface significantly reduces PEI dose (PEI/siRNA weight ratio) compared to free PEI and to covalently PEI-modified SiO_2 NPs[31] by introducing a new additional form of bonding between siRNA species and the delivery nanocarrier system. Using higher Ce^{3+} surface amounts (like in SPA-Ce_{60}-PEI NPs) slightly reduces both silencing and cytotoxic effects by increasing neutralization of PEI amine functions. Accordingly, we believe that this approach might be a quite powerful possibility for nanocarrier dosage reduction via metal cation-modified 25 kDa *b*-PEI. To reduce the cytotoxicity of such a system in the near future, the covalent attachment of Ce^{3+}-binding **N**-based ligands through primary amines will stabilize the binding between both polymer phase and Ce^{3+} cations/complexes enabling (i) a reduced composite cytotoxicity along with (ii) securing the overall silencing features of such a *b*-PEI complexed phase.

■ EXPERIMENTAL SECTION

Materials. Tetraethyl orthosilicate (TEOS, 99.999%), ammonium hydroxide (ACS reagent, 28−30%), polyethylenimine (25 kDa branched PEI, MW ∼25 000 Da), cerium(III) chloride heptahydrate ($CeCl_3{\cdot}7H_2O$, 99%), and triethylamine (Et_3N, ≥99%) were purchased from Sigma-Aldrich (Israel). 3-Aminopropyl-triethoxysilane (APTES, 99%) was purchased from Acros Organics. All experiments and analyses used deionized water. All chemicals and solvents were reagent grade and were used without any further purification or modification.

Synthesis of PolyNH_2−SiO_2 (SPA) NPs by the Stöber Process. SiO_2 NPs were synthesized by a general method that includes hydrolysis and further condensation of the silicate source (TEOS) in EtOH under basic conditions. The exact procedure included dissolution of ammonium hydroxide (2.4 mL, ∼18 mmol) in absolute ethanol (60 mL) followed by addition of TEOS (2.4 mL, 10.7 mmol). The reaction was stirred overnight at ambient temperature until formation of NPs was complete, followed by addition of APTES (300 μL, 1.28 mmol); the reaction was then stirred for another 24 h. The resulting polyNH_2−SiO_2 NPs (SPA NPs) were cleaned to remove excess ammonium hydroxide and other compounds/contaminants by repeated centrifugation (12 min, 13 500 rpm, ∼19 500 *g*-force, 4 °C) and redispersion in a 1:1 v/v H_2O−EtOH mixture for three cycles, followed by the same action with H_2O (2−3 times).

Synthesis of SPA-Ce-PEI NPs. To a series of sonicated (5 min in Elmasonic s 30 ultrasonic bath, 37 kHz) dispersions of SPA NPs (100 mg each, 0.5 mmol $-NH_2$ groups/g SPA NPs) in H_2O replaced in 50 mL bottles, NEt_3 (25 μL, 0.18 mmol) was added and vortexed. Then, aliquots of a $CeCl_3{\cdot}7H_2O$ solution (10 mM) were added (1 and 3 mL that were corresponding for 10 and 30 μmol, respectively) to the vessels for obtaining 20 and 60 mol % of surface primary amines. All the samples were brought to the same total volume of 20 mL by addition of deionized H_2O. After 3 h stirring at ambient temperature, reagents in excess were washed by three cycles of centrifugation (12 min, 13 500 rpm, ∼19 500 *g*-force, 4 °C), and the modified SiO_2−Ce (SPA-Ce) NPs were redispersed in H_2O (5 mL). An aliquot (1.5 mL, 30 mg) was taken from each vessel for NP analysis (ICP-AES and TGA).

To the remaining NPs (3.5 mL, 70 mg), NEt_3 (15.4 μL, 0.11 mmol) and aqueous 25 kDa PEI solution (10 mg/mL, 1.4 mL) were added. Each sample was brought to total volume of 14 mL by H_2O addition. Reactions were allowed to stir at ambient temperature overnight and then excess of PEI and NEt_3 was washed by centrifugation (12 min, 13 500 rpm, 4 °C) and redispersion in H_2O three times.

Physicochemical Characterization. The following properties of SiO_2 NPs were characterized: size, shape, surface charge, Ce weight percentage (by inductively coupled plasma atomic emission spectroscopy, ICP-AES), and amount of organic matter (by thermogravimetric analysis, TGA).

Transmission Electron Microscopy. The size and shape of nanoparticles were obtained by using a high resolution transmission microscopy (JEM 2100, JEOL USA Inc.) equipped with a CCD 4 × 4k camera (Gatan) have been used. Samples for TEM imaging were prepared by placing a drop of diluted EtOH dispersion (200−250 μg/mL) onto a 400-mesh copper TEM grid (400C-FC, Electron Microscopy Sciences, Hatfield, PA, USA) and then drying at vacuum chamber at ambient temperature.

DLS and ζ Potential. The hydrodynamic size and surface charge of NPs in dispersion were measured by a ZetaSizer Nano-ZS (Malvern Instruments Ltd., Worcestershire, UK). Size measurements were performed by dynamic light scattering (DLS) of dilute nanoparticle aqueous dispersions (∼0.05 mg/mL). The samples were sonicated for 5 min before analysis. The ZetaSizer Nano series was also used to determine the ζ potential of NPs by measuring NP electrophoretic mobility and then applying the Henry equation.[37]

Inductively Coupled Plasma Atomic Emission Spectroscopy (ICP-AES). Amounts of Ce metal ions were measured using an ICP-AES ULTIMA 2 spectrometer (HORIBA, Jobin Yvon Inc.). To analyze metal amounts, dry powder samples (2−4 mg) were dissolved in concentrated HCl (∼0.5 mL) at ambient

DOI: 10.1021/acs.bioconjchem.5b00100
Bioconjugate Chem. 2015, 26, 880−889

temperature and diluted with H_2O to a known volume (5 or 10 mL) using a volumetric flask. This treatment does not fully dissolve SiO_2 NPs but releases all Ce cations from their solid matrix into solution. Filtration of the solution through a Millipore filter (Nylon, 0.22 μm) is highly required before ICP analysis. A classic calibration method with standard solutions of elemental Ce was used to quantify metal amounts.

Thermogravimetric Analysis (TGA). TGA analyses were performed by using a TGA/DSC1 analyzer (Mettler-Toledo, OH, USA) for which dry NPs samples (8−10 mg) were taken. Thermograms were recorded in air at a heating rate of 10 °C min^{-1} over a 25−800 °C temperature range.

Characterization of SPA-Ce-PEI/siRNA Polyplexes by DLS and ζ Potential Measurements. To obtain the size and ζ potential of SPA-Ce-PEI/siRNA polyplexes with different weight ratios, a series of dispersions was prepared in the following manner. The addition of varied amounts of siRNA (24.3, 12.1, 8.1, 6.1, 4.9, and 2.4 μg) into a constant amount of SPA-Ce-PEI NPs (50 μg) gave a series of various PEI/siRNA w/w ratios (0.2, 0.4, 0.6, 0.8, 1.0, and 2.0). The polyplexes were allowed to form (15 min, ambient temperature), and H_2O was added to each sample up to 1 mL of a total volume. A sample without siRNA was also prepared by the same manner. Size and ζ potential were measured for each sample in triplicate repetition mode.

Cell Culture. The dual luciferase-expressing U2OS human osteosarcoma cell line was generated as previously described.[31] Cells were cultured in Dulbecco's Modified Eagle Medium supplemented with 10% fetal bovine serum, 100 μg/mL penicillin, 100 U/mL streptomycin, and 2 mM L-glutamine (Biological Industries Ltd., Israel) and grown at 37 °C with 5% CO_2. Incubations of cells with or without any additive were performed in similar conditions unless otherwise stated.

MTT Toxicity Assay. U2OS-Luc cells were seeded (1×10^4 cells/well) in a 96 well plate (Greiner) and incubated overnight. Cells were treated with Firefly luciferase siRNA (0.166 μg, 100 nM) bound to different NPs at different PEI/siRNA w/w ratios. Alternatively, cells were treated with different concentrations of NPs, PEI, or $CeCl_3 \cdot 7H_2O$ (see the SI section). Cells without treatment were used as a control. After 48 h incubation, the medium was removed, and 100 μL of fresh medium containing the MTT reagent (3-[4,5-dimethylthiazol-2-yl]-2,5-diphenyltetrazolium bromide, Sigma-Aldrich) (0.5 mg/mL) was added to each well followed by 20 min incubation. After incubation, MTT was removed, and 50 μL of DMSO (Sigma-Aldrich) was added to each well. All the absorption values were measured at 570 nm (Synergy 4, Biotek) and normalized to control.

Endocytosis of SPA-Ce-PEI/FITC-siRNA Polyplexes. U2OS-Luc cells were seeded (1×10^5 cells/well) in a 12 well plate (Greiner) with coverslips and incubated overnight. Cells were transfected with siGLO Green Transfection Indicator (50 nM) (FITC) (Dharmacon) mixed with SPA-Ce_{60}-PEI NPs at a 0.6 PEI/siRNA w/w ratio. After 24 h, cells were fixed with paraformaldehyde solution (4% in PBS) (Santa Cruz Biotechnology) for 20 min at RT and nuclei were stained with DAPI solution (1 μg/mL in PBS) (blue) (Sigma) for 10 min at RT. Images were taken with a Leica TCS SPE (63×) confocal laser scanning microscope (CLSM), and then, the 3D images were edited in the software *Imaris* (Bitplane).

Luciferase Assay. U2OS-Luc cells were seeded (1×10^4 cells/well) in a 96 well optical bottom plate (Thermo) and incubated overnight. Cells were transfected with Firefly luciferase siRNA (0.166 μg, 100 nM) bound to different NPs or PEI polymer at different PEI/siRNA w/w ratios or without treatment (control). After 48 h, cells were assayed for both Firefly and *Renilla* luciferase activities using the Dual Luciferase Assay System (Promega). Briefly, cells were lysed and the Firefly luciferase substrate added (50 μL per well Dual Substrate/Buffer). Firefly luciferase activity was measured after 10 min using a luminometer (Synergy 4, Biotek). Next, the *Renilla* luciferase substrate was added (50 μL per well Stop & GLO Substrate/Buffer) and the luminescence measured after a further 10 min of incubation. Silencing efficacy was reflected by luciferase activities normalized to control luciferase activities.

The following oligonucleotide sequences (sense/antisense) were used: 5′-GGACAUCACCUAUGCCGAGUACUTC-3′/5′-CACCUGUAGUGGAUACGGCUCA UGAAG-3′ (IDT Technologies, Coralville, IA).

■ ASSOCIATED CONTENT

Supporting Information

Dynamic Light Scattering (DLS). ζ potential measurements. Cytotoxicity results (MTT assays). Gene silencing results (Luciferase assay). This material is available free of charge via the Internet at http://pubs.acs.org/

■ AUTHOR INFORMATION

Corresponding Authors

*E-mail: michaes@mail.biu.ac.il. Tel.: +972 3 531 8068. Fax: +972 3 535 1824.

*E-mail: jean-paul.m.lellouche@biu.ac.il. Tel.: +972 3 531 8324. Fax: +972 3 738 4053.

Author Contributions

#All the authors contributed equally to this work.

Notes

The authors declare no competing financial interest.

■ ACKNOWLEDGMENTS

The authors would like to thank Bar-Ilan University for funding this project, Drs. Luba Burlaka and Ilana Perelshtein for taking TEM images, and Drs. Ortal Haik and Yaffa Pinkhas for operating the ICP-AES instrumentation.

■ REFERENCES

(1) Campbell, T. N., and Choy, F. Y. M. (2005) RNA interference: past, present and future. *Curr. Issues Mol. Biol. 7*, 1−6.

(2) Fire, A., Xu, S., Montgomery, M. K., Kostas, S. A., Driver, S. E., and Mello, C. C. (1998) Potent and specific genetic interference by double-stranded RNA in Caenorhabditis elegans. *Nature 391*, 806−811.

(3) Hammond, S. M., Boettcher, S., Caudy, A. A., Kobayashi, R., and Hannon, G. J. (2001) Argonaute2, a link between genetic and biochemical analyses of RNAi. *Science 293*, 1146−1150.

(4) Pecot, C. V., Calin, G. A., Coleman, R. L., Lopez-Berestein, G., and Sood, A. K. (2011) RNA interference in the clinic: challenges and future directions. *Nat. Rev. Cancer 11*, 59−67.

(5) Elbashir, S. M., Harborth, J., Lendeckel, W., Yalcin, A., Weber, K., and Tuschl, T. (2001) Duplexes of 21-nucleotide RNAs mediate RNA interference in cultured mammalian cells. *Nature 411*, 494−498.

(6) Angart, P., Vocelle, D., Chan, C., and Walton, S. P. (2013) Design of siRNA therapeutics from the molecular scale. *Pharmaceuticals 6*, 440−468.

(7) Aleman, L. M., Doench, J., and Sharp, P. A. (2007) Comparison of siRNA-induced off-target RNA and protein effects. *RNA 13*, 385−395.

DOI: 10.1021/acs.bioconjchem.5b00100
Bioconjugate Chem. 2015, 26, 880−889

(8) Jackson, A. L., Burchard, J., Schelter, J., Chau, B. N., Cleary, M., Lim, L., and Linsley, P. S. (2006) Widespread siRNA "off-target" transcript silencing mediated by seed region sequence complementarity. *RNA 12*, 1179−1187.
(9) Aigner, A. (2008) Cellular delivery in vivo of siRNA-based therapeutics. *Curr. Pharm. Des. 14*, 3603−3619.
(10) Wang, Y., Li, Z., Han, Y., Liang, L. H., and Ji, A. (2010) Nanoparticle-based delivery system for application of siRNA in vivo. *Curr. Drug Metab. 11*, 182−196.
(11) Günther, M., Lipka, J., Malek, A., Gutsch, D., Kreyling, W., and Aigner, A. (2011) Polyethylenimines for RNAi-mediated gene targeting in vivo and siRNA delivery to the lung. *Eur. J. Pharm. Biopharm. 77*, 438−449.
(12) Richards Grayson, A., Doody, A., and Putnam, D. (2006) Biophysical and structural characterization of polyethylenimine-mediated siRNA delivery in vitro. *Pharm. Res. 23*, 1868−1876.
(13) Akinc, A., Thomas, M., Klibanov, A. M., and Langer, R. (2005) Exploring polyethylenimine-mediated DNA transfection and the proton sponge hypothesis. *J. Gene Med. 7*, 657−663.
(14) Won, Y.-Y., Sharma, R., and Konieczny, S. F. (2009) Missing pieces in understanding the intracellular trafficking of polycation/DNA complexes. *J. Controlled Release 139*, 88−93.
(15) Guenther, M., Lipka, J., Malek, A., Gutsch, D., Kreyling, W., and Aigner, A. (2011) Polyethylenimines for RNAi-mediated gene targeting in vivo and siRNA delivery to the lung. *Eur. J. Pharm. Biopharm. 77*, 438−449.
(16) Nimesh, S. (2012) Polyethylenimine as a promising vector for targeted siRNA delivery. *Curr. Clin. Pharmacol. 7*, 121−130.
(17) Vicennati, P., Giuliano, A., Ortaggi, G., and Masotti, A. (2008) Polyethylenimine in medicinal chemistry. *Curr. Med. Chem. 15*, 2826−2839.
(18) Aravindan, L., Bicknell, K. A., Brooks, G., Khutoryanskiy, V. V., and Williams, A. C. (2013) A comparison of thiolated and disulfide-crosslinked polyethylenimine for nonviral gene delivery. *Macromol. Biosci. 13*, 1163−1173.
(19) Cheng, W., Yang, C., Hedrick, J. L., Williams, D. F., Yang, Y. Y., and Ashton-Rickardt, P. G. (2013) Delivery of a granzyme B inhibitor gene using carbamate-mannose modified PEI protects against cytotoxic lymphocyte killing. *Biomaterials 34*, 3697−3705.
(20) Lo, Y.-L., Sung, K.-H., Chiu, C.-C., and Wang, L.-F. (2013) Chemically conjugating polyethylenimine with chondroitin sulfate to promote CD44-mediated endocytosis for gene delivery. *Mol. Pharmaceutics 10*, 664−676.
(21) Tian, H., Li, F., Chen, J., Huang, Y., and Chen, X. (2012) N-Isopropylacrylamide-modified polyethylenimines as effective gene carriers. *Macromol. Biosci. 12*, 1680−1688.
(22) Tripathi, S. K., Singh, V. P., Gupta, K. C., and Kumar, P. (2013) Hydrophobic and membrane permeable polyethylenimine nanoparticles efficiently deliver nucleic acids in vitro and in vivo. *J. Mater. Chem. B1*, 2515−2524.
(23) Wen, S., Zheng, F., Shen, M., and Shi, X. (2013) Surface modification and PEGylation of branched polyethyleneimine for improved biocompatibility. *J. Appl. Polym. Sci. 128*, 3807−3813.
(24) Anwander, R. (1999) Principles in Organolanthanide Chemistry. In *Lanthanides: Chemistry and Use in Organic Synthesis* (Kobayashi, S., Ed.) pp 4−7, 36, 37, Springer, Berlin.
(25) Cotton, F. A., Wilkinson, G., Murillo, C. A., and Bochmann, M. (1999) *Advanced Inorganic Chemistry*, 6th ed., Wiley-Interscience, New York.
(26) Mingos, D. M. P. (1998) *Essential Trends in Inorganic Chemistry*, Oxford University Press, New York.
(27) Karraker, D. G. (1970) Coordination of trivalent lanthanide ions. *J. Chem. Educ. 47*, 424−430.
(28) Pearson, R. G. (1969) Hard and Soft Acids and Bases. In *Survey of Progress in Chemistry* (Scott, A. F., Ed.) pp 12−13, Academic Press, New York.
(29) Belfiore, L. A., Ruzmaikina, I. Y., and Das, P. K. (2001) Thermophysical property modifications in functional polymers via lanthanide trichloride hydrates. *Polym. Eng. Sci. 41*, 1196−1205.
(30) Stöber, W., Fink, A., and Bohn, E. (1968) Controlled growth of monodisperse silica spheres in the micron size range. *J. Colloid Interface Sci. 26*, 62−69.
(31) Kapilov Buchman, Y., Lellouche, E., Zigdon, S., Bechor, M., Michaeli, S., and Lellouche, J.-P. (2013) Silica nanoparticles and polyethyleneimine (PEI)-mediated functionalization: a new method of PEI covalent attachment for siRNA delivery applications. *Bioconjugate Chem. 24*, 2076−2087.
(32) Sarin, V. K., Kent, S. B. H., Tam, J. P., and Merrifield, R. B. (1981) Quantitative monitoring of solid-phase peptide synthesis by the ninhydrin reaction. *Anal. Biochem. 117*, 147−157.
(33) Chen, Y., Lian, G., Liao, C., Wang, W., Zeng, L., Qian, C., Huang, K., and Shuai, X. (2013) Characterization of polyethylene glycol-grafted polyethylenimine and superparamagnetic iron oxide nanoparticles (PEG-g-PEI-SPION) as an MRI-visible vector for siRNA delivery in gastric cancer in vitro and in vivo. *J. Gastroenterol. 48*, 809−821.
(34) Dong, D.-W., Xiang, B., Gao, W., Yang, Z.-Z., Li, J.-Q., and Qi, X.-R. (2013) pH-responsive complexes using prefunctionalized polymers for synchronous delivery of doxorubicin and siRNA to cancer cells. *Biomaterials 34*, 4849−4859.
(35) Liu, G., Xie, J., Zhang, F., Wang, Z., Luo, K., Zhu, L., Quan, Q., Niu, G., Lee, S., Ai, H., et al. (2011) N-Alkyl-PEI-functionalized iron oxide nanoclusters for efficient siRNA delivery. *Small 7*, 2742−2749.
(36) Wu, C., Gong, F., Pang, P., Shen, M., Zhu, K., Cheng, D., Liu, Z., and Shan, H. (2013) An RGD-modified MRI-visible polymeric vector for targeted siRNA delivery to hepatocellular carcinoma in nude mice. *PLoS One 8*, e66416.
(37) Hunter, R. J. (1981) *Zeta Potential in Colloid Science: Principles and Applications*, Academic Press, New York.

DOI: 10.1021/acs.bioconjchem.5b00100
Bioconjugate Chem. 2015, 26, 880−889